Production of ultracold ground-state LiRb molecules by photoassociation through a resonantly coupled state

I. C. Stevenson,[1] D. B. Blasing,[2] Y. P. Chen,[1,2,3] and D. S. Elliott[1,2,3]

[1]*School of Electrical and Computer Engineering, Purdue University, West Lafayette, Indiana 47907, USA*

[2]*Department of Physics and Astronomy, Purdue University, West Lafayette, Indiana 47907, USA*

[3]*Purdue Quantum Center, Purdue University, West Lafayette, Indiana 47907, USA*

We report on a resonantly coupled 2(1)-4(1) photoassociation resonance in LiRb. This pair of states displays interesting decay physics that hint at interference-like effects caused by two different decay paths. We observe decay to predominantly $X\,^1\Sigma^+$ $v = 43$, with significant numbers of molecules produced in $X\,^1\Sigma^+$ $v = 2-12$. This photoassociation resonance also produces $\sim$300 $X\,^1\Sigma^+$ $v = 0$ $J = 0$ molecules/s. Finally, we identify a stimulated Raman adiabatic passage transfer pathway from $v = 43$ to $v = 0$ that has the potential to produce up to 2×10^5 LiRb molecules/s in the $X\,^1\Sigma^+$ $v = 0$ $J = 0$ state.

I. INTRODUCTION

Ultracold polar molecules are interesting for many reasons [1–3]. In particular, their permanent electric dipole moment in the rovibronic ground state produces unique physical interactions [4–6]. To realize many of these goals, a continuous means of generating a high density sample of rovibronically cold dipolar molecules would be very useful. Currently, the most successful polar molecule experiments use an experimentally challenging pulsed technique. Molecules are produced via magnetoassociation and transfered to the rovibronic ground state (that is vibrational, rotational, and electronic ground state) with stimulated Raman adiabatic passage (STIRAP) [7]. However, ground-state generation by direct spontaneous emission after photoassociation (PA) has been observed previously in homonuclear molecules [8,9], KRb [10], LiCs [11], RbCs [12], and NaCs [13], and explored theoretically in Ref. [14]. This method is experimentally simpler and continuous. There have been several proposals for trapping these continuously generated ground-state molecules [12,15] and several for increasing the phase-space density to be competitive with the pulsed production method [16–18]. For the continuous generation method to be successful, a PA resonance that produces large numbers of cold molecules, preferably in one vibrational state, is essential.

In this work, we investigate a newly discovered photoassociation resonance, a mixed state consisting of resonantly coupled 2(1)-4(1) long-range states in LiRb that produces large numbers of deeply bound molecules. Similar resonantly coupled states exist in other molecules [10,13,14] and spontaneous decay to the electronic $X\,^1\Sigma^+$ ground state, including the lowest vibrational state, has been observed; we find this holds true for LiRb. Molecules associated through this resonance decay to many vibrational levels of both the $X\,^1\Sigma^+$ ground state and the $a\,^3\Sigma^+$ lowest triplet state, with nearly half of these molecules decaying to $X\,^1\Sigma^+$ $v = 43$. We use resonantly enhanced multiphoton ionization (REMPI) and a type of depletion spectroscopy to explore the production rate and distribution of the molecules; because of its strong decay to stable molecular states, we have found this PA resonance to be a very successful platform to study bound-to-bound transitions in LiRb [19]. Finally, as part of this work we

present observations of ultracold $X\,^1\Sigma^+$ $v = 0$ $J = 0$ LiRb molecules formed at around 300 molecules/s and discuss plans for producing up to 2×10^5 rovibronic ground states molecules/s. The relevant potential-energy curves (PEC) for these measurements are in Fig. 1.

II. EXPERIMENTAL PARAMETERS

The details of our experimental apparatus are described elsewhere [20] so we provide only a brief summary. We work out of a dual-species MOT, $\lesssim$1 mK in temperature and 1 mm in diameter [21], trapping $\sim$5$\times10^7$ ^{7}Li atoms and $\sim10^8$ ^{85}Rb atoms. Our Rb MOT is a spatial dark spot MOT [22]. We photoassociate Li and Rb atoms using the output of either a 300 mW cw Ti:sapphire laser, or a 150 mW external-cavity diode laser (ECDL) tuned below the Rb D_1 asymptote at 795 nm. The beams are collimated to a $1/e^2$ diameter of 0.7 mm at the center of the MOTs. We ionize the molecules that decay from the PA state to the $X\,^1\Sigma^+$ or $a\,^3\Sigma^+$ electronic states with the REMPI process driven by a Nd:YAG pumped pulsed dye laser, tunable in the wavelength range between 550 and 583 nm ($18150-17150\,\mathrm{cm}^{-1}$). The repetition rate of this laser is 10 Hz, and it delivers $\sim$3 mJ/pulse to the MOT region in a 4 mm diameter beam. When one-photon of this laser is resonant with a transition from an initial state (populated by spontaneous decay from the PA state) to an intermediate bound state (usually one of the vibrational levels of the $B\,^1\Pi$, $D\,^1\Pi$, $f\,^3\Pi$, or $g\,^3\Sigma^+$ electronic potentials, not shown in Fig. 1), then the molecule may absorb two photons and ionize. We detect and count LiRb$^+$ ions using a time-of-flight spectrometer and a microchannel plate detector. To observe ions from deeply bound states we use a two-color variant of REMPI called RE2PI. In RE2PI we reduced the power of the dye laser pulse, and used the energetically higher photon from the 532 nm second-harmonic output of the Nd:YAG as the second photon. Our notation is as follows: v'' and J'' denote the vibrational and rotational levels of the $X\,^1\Sigma^+$ and $a\,^3\Sigma^+$ states, v and J denote the vibrational and rotational levels of the electronically excited states driven by PA resonances (and for these vibrational numbers, we count down from the asymptote using negative integers), and v' and
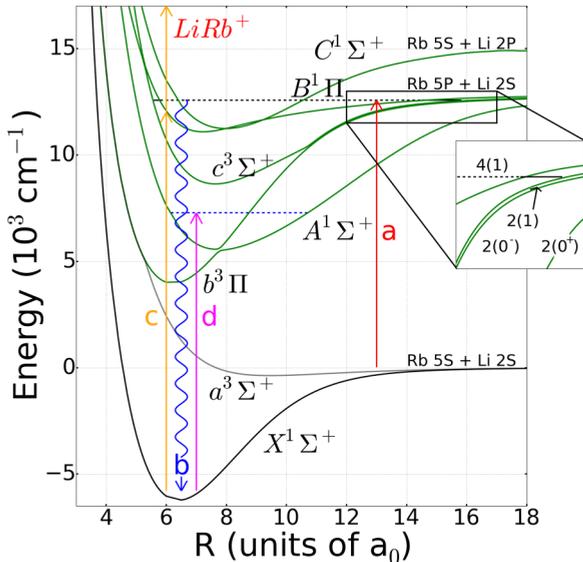
FIG. 1. Low-lying PEC diagram for the LiRb molecule from Ref. [23]. Vertical lines show various optical transitions, including (a) photoassociation of molecules below the Rb D_1 asymptote, at frequency ν_a, (b) spontaneous decay of excited state molecules leading to $X\,^1\Sigma^+$ (and $a\,^3\Sigma^+$), (c) REMPI or RE2PI to ionize LiRb molecules, at frequency ν_c, and (d) state-selective excitation to deplete the REMPI signal, at frequency ν_d. The black and blue dashed lines respectively represent our 2(1)–4(1) mixed states and our depletion state. The inset shows an expanded view of the long-range potentials near the asymptote. Table I shows the correlation between long-range and short-range labeling.

J' denote vibrational and rotational labeling of other excited electronic states. Additionally, we use Hund's case (c) labeling for PA states and Hund's case (a) labeling for deeply bound states. The correspondence between the two labeling schemes is shown in Table I. The PA state that is central to much of this work has two equivalent notations: 4(1) $v = -16$ in Hund's case (c) notation and $B\,^1\Pi\ v' = 20$ in Hund's case (a) notation. We will label this state using Hund's case (c) notation for consistency with the usual practice for long-range PA states although the state lives somewhere between the two Hund's cases.

TABLE I. Correspondence between Hund's cases (a) and (c) in LiRb. We use Hund's case (c) labeling for our PA states and Hund's case (a) for deeply bound state. Note that $B\,^1\Pi\ v' = 20$ and 4(1) $v = -16$ denote the same state.

Hund's case (a)	Hund's case (c)	Atomic asymptote
$A\,^1\Sigma^+$	$2(0^+)$	Rb $^5P_{1/2}$ +Li $2S$
$c\,^3\Sigma^+$	$2(0^-)$	
	$2(1)$	
$b\,^3\Pi$	$3(0^+)$	Rb $^5P_{3/2}$ +Li $2S$
	$3(0^-)$	
	$3(1)$	
	$1(2)$	
$B\,^1\Pi$	$4(1)$	

III. RESONANT COUPLING EVIDENCE

In Fig. 2(a) we show the PA spectrum of the 2(1)-4(1) mixed states near 122 GHz below the D_1 asymptote. For this spectrum the REMPI laser frequency, ν_c, was fixed on the $D\,^1\Pi\ v' = 4 \leftarrow X\,^1\Sigma^+\ v'' = 10$ transition and the PA laser frequency, ν_a, was scanned. The 4(1) $v = -16\ J = 1$ and 2(1) $v = -5\ J = 1$ states in this spectrum are coupled [24], forming mixed states that possess characteristics of each [25], namely, the good photoassociation strength of a 2(1) state and the deep decay path of a 4(1) state. Coupling and mixing between vibrational levels of different electronic states can occur when states with the same rotational number J and angular momentum Ω lie close energetically [10,26]. Ω is the projection of the total angular momentum (excluding nuclear spin) onto the internuclear axis. Figure 2(a) contains several hyperfine echoes, labeled with ⋆ for Li $F = 1$, Rb $F = 2$; △ for Li $F = 2$, Rb $F = 3$; and ⋄ for Li $F = 1$, Rb $F = 3$. These are weaker PA lines that originate from population in our MOTs not in our main hyperfine component.

There are three features in Fig. 2 that provide evidence of resonant coupling of the 2(1) and 4(1) states.

(a) A 2(1) component is indicated by the large photoassociation amplitude of the 4(1) $v = -16$ state. We previously explored the $v = -3, -4$, and -5 lines of the 4(1) state [27], and found that the photoassociation amplitude for any vibrational levels more deeply bound than $v = -6$ had vanished. The enhanced photoassociation amplitude for 4(1) $v = -16$, with no visible photoassociation at $v = -15$ and $v = -17$, is an indication of mixing with a 2(1) state.

(b) The frequency spacing between the $J = 1$ and $J = 2$ lines of the 4(1) $v = -16$ state in Fig. 2(a) is increased by $\sim$1 GHz from the spacing expected based on earlier spectroscopy of LiRb [28] that studied highly excited rotational states of the 4(1) $v = -16$ manifold. We have marked the expected spacing between the $J = 1$ and 2 lines with vertical dashed red lines using $B_v = 2.503\ (0.001)$ GHz [28]. We expect the $J = 2$ state to be relatively unperturbed because it is much farther from the perturbing 2(1) state.

(c) Further evidence of 2(1)-4(1) mixing is given in the REMPI spectra shown in Fig. 2(b). These provide an indirect measure of the relative spontaneous decay paths after photoassociation. We recorded these spectra by tuning the PA laser to the 4(1) $v = -16\ J = 1$ line (blue solid spectrum) or the 2(1) $v = -5\ J = 1$ (red dot-dashed spectrum). We have identified and labeled the lines in these spectra, and found population in vibrational levels of the $X\,^1\Sigma^+$ and $a\,^3\Sigma^+$ electronic potentials. Previously we observed that other 2(1) states decay only to $a\,^3\Sigma^+$ states, while other 4(1) states decay solely to $X\,^1\Sigma^+$ states [21,27]. However, the 4(1) $v = -16\ J = 1$ and the 2(1) $v = -5\ J = 1$ states decay to both $X\,^1\Sigma^+$ and $a\,^3\Sigma^+$, providing further evidence of their coupling.

Our current and previous spectroscopy on 4(1) $v = -16$ state allows us to analyze two interesting spectroscopic quantities of LiRb. First, this leads us to a higher precision determination of the dissociation energy, D_e, of the $X\,^1\Sigma^+$ potential. We use the transition frequency of the $B\,^1\Pi\ v' = 20 \leftarrow X\,^1\Sigma^+\ v'' = 0$ transition from Ref. [28], the PA frequency of the 4(1) $v = -16\ J = 2$ peak in Fig. 2(a),
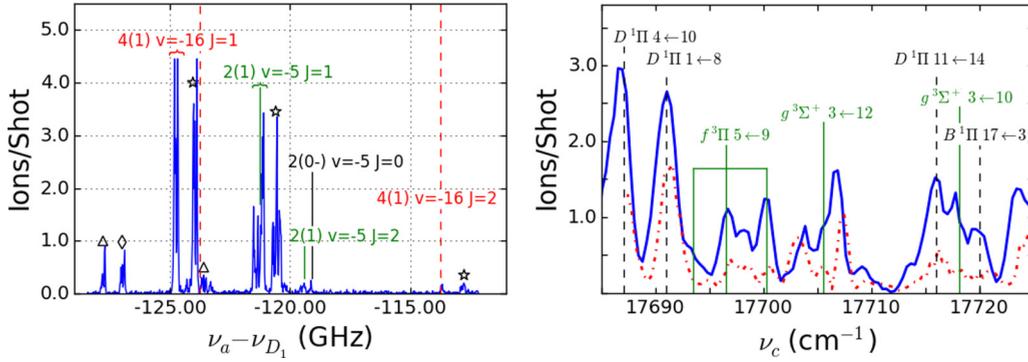
FIG. 2. Evidence of 2(1)-4(1) mixing. (a) PA spectrum of the 2(1)-4(1) mixed states. The REMPI laser frequency was held fixed at 17,686.8 cm^{-1} on the $D\,^1\Pi\ v' = 4 \leftarrow v'' = 10$ transition. Hyperfine echoes are labeled by $\star$ for Li $F = 1$, Rb $F = 2$, $\triangle$ for Li $F = 2$, Rb $F = 3$, and $\diamond$ for Li $F = 1$, Rb $F = 3$. New 4(1) resonances as well as previously observed 2(1) and 2(0$^-$) are labeled [21]. Dashed lines show the expected rotational spacing of the 4(1) lines based on previous work [28]. (b) REMPI spectra from photoassociation through the 4(1) and 2(1) states; (blue solid) 4(1) $v = -16$ $J = 1$, (red dot-dashed) 2(1) $v = -5$ $J = 1$. The black dashed vertical lines represent transitions out of $X\,^1\Sigma^+$ and the green solid vertical lines are transitions out of $a\,^3\Sigma^+$; labeling is $v'' \rightarrow$ (excited state) v'.

measured to be 12575.21 (0.02) cm^{-1}, the rotational constant of the $B\,^1\Pi\ v' = 20$ state also from Ref. [28], and the ground-state molecular constants from Ref. [29]. This allows us to report a $X\,^1\Sigma^+$ dissociation energy of 5928.08 (0.03) cm^{-1} relative to the ^{85}Rb $5s\,^2S_{1/2}\ F = 2 + {}^7$Li $2s\,^2S_{1/2}\ F = 1$ asymptote. This determination agrees with, but is of much greater precision than, the previous value of 5927.9 (4.0) cm^{-1} [29].

We can also use this PA spectrum to estimate the admixture coefficients of the 2(1)-4(1) $J = 1$ states. We write the mixed states $|\Psi_-\rangle$ [primarily 4(1) $J = 1$] and $|\Psi_+\rangle$ [primarily 2(1) $J = 1$] as

$$|\Psi_-\rangle = c|\Psi_{4(1)}\rangle - d|\Psi_{2(1)}\rangle, \quad \text{with energy } E_-, \quad (1)$$

and

$$|\Psi_+\rangle = d|\Psi_{4(1)}\rangle + c|\Psi_{2(1)}\rangle, \quad \text{with energy } E_+, \quad (2)$$

where $|\Psi_{4(1)}\rangle$ and $|\Psi_{2(1)}\rangle$ are the bare (unmixed) states with energies $E_{4(1)}$ and $E_{2(1)}$, respectively. We refer the reader to the treatment of resonantly coupled rotational states in Ref. [26]. We measure the frequency difference of the perturbed states to be $(E_+ - E_-)/h = 3.5$ (0.1) GHz, as shown in the PA spectra of Fig. 2(a). As discussed earlier, we know the size of the perturbation on the 4(1) state based on the deviation from the rotational constant for this state measured by Ref. [28]. Assuming an equal but opposite shift in the 2(1) energy, we find the energy difference of the unperturbed states to be $\delta = (E_{2(1)} - E_{4(1)})/h = 1.5$ (0.2) GHz. Following the treatment of Ref. [26], we can use the perturbed and unperturbed energy spacings to derive the coupling between the states, V_{int}, by diagonalizing a simple 2×2 matrix,

$$\begin{vmatrix} E_{2(1)} - E & V_{\text{int}} \\ V_{\text{int}} & E_{4(1)} - E \end{vmatrix} = 0.$$

This will have solutions

$$E_\pm = \tfrac{1}{2}(E_{2(1)} + E_{4(1)}) \pm \tfrac{1}{2}\sqrt{4|V_{\text{int}}|^2 + \delta^2}. \quad (3)$$

Re-solving this for the state coupling yields $V_{\text{int}} = \tfrac{1}{2}\sqrt{(E_+ - E_-)^2 - \delta^2} = 1.6$ (0.2) GHz. Additionally we can find the eigenstates of our diagonalized matrix to find the

admixture coefficients $|c| = 0.84$ (0.09) and $|d| = 0.53$ (0.05), consistent with our earlier assertion of strong mixing between the states.

IV. RELATIVE DECAY PATHS

To supplement the PA spectra discussed above, we have also observed the 4(1)-2(1) $J = 1$ mixed resonance through trap loss measurements. We show these spectra in Fig. 3. In contrast to the REMPI signal, which indicates formation of a stable molecule in a specific vibrational level of the $X\,^1\Sigma^+$ or $a\,^3\Sigma^+$ state, a dip in the trap fluorescence signal results when the PA laser associates a molecule, regardless of whether that molecule decays to a stable state or to a pair of free atoms. An interesting feature of these spectra is that the $|\psi_+\rangle$ PA resonance, whose primary constituent is the bare 2(1) $v = -5$ $J = 1$ state, is stronger in trap loss (22% trap loss) than the $|\psi_-\rangle$ line (12% trap loss), while the $|\psi_-\rangle$ resonance is
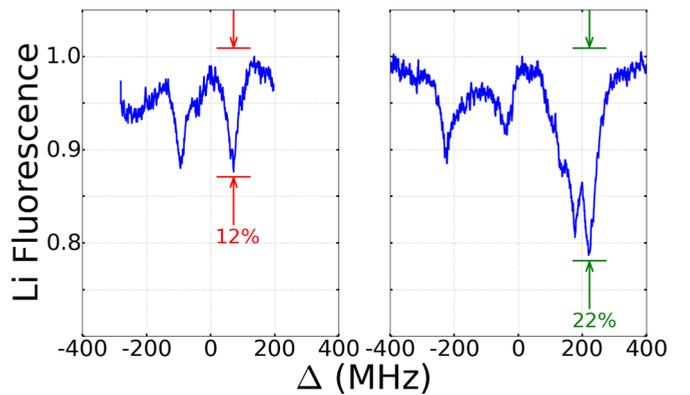

FIG. 3. Trap loss spectroscopy of 4(1) $v = -16$ $J = 1$ (left) and 2(1) $v = -5$ $J = 1$ (right) PA resonances. Detuning is relative to the assigned PA line center. Notice the relative strength favoring the 2(1) resonance in contrast to the REMPI data in Fig. 2(a). More details on our trap loss experiments can be found in Ref. [30]. The structure in these spectra is caused by the hyperfine structure of the 4(1) and 2(1) states.

TABLE II. Enhancement of decay of $|\Psi_-\rangle$ across several vibrational levels.

	$\frac{R_{CM}^-}{R_{CM}^+}$	$\frac{B^+(v'')}{B^-(v'')}$	$\mathcal{R}(v'')$	$c^2\,\mathcal{R}^2(v'')$	$2cd\mathcal{R}(v'')$	d^2	$B^+(v'')$	$d^2\,\mathcal{R}^2(v'')$	$-2cd\mathcal{R}(v'')$	c^2	$B^-(v'')$
$X\,^1\Sigma^+\;v''=2$	2.5 (0.1)	4.6	-0.13 (0.05)	0.01	-0.12	0.29	0.18	0.00	0.12	0.71	0.83
$a\,^3\Sigma^+\;v''=7$	1.5 (0.1)	2.8	-0.02 (0.05)	0.00	-0.02	0.29	0.27	0.00	0.02	0.71	0.73
$X\,^1\Sigma^+\;v''=43$	2.2 (0.3)	4.0	-0.10 (0.05)	0.01	-0.09	0.29	0.20	0.00	0.09	0.71	0.80

stronger than $|\psi_+\rangle$ in the REMPI spectra. In the following, we apply a simple model to characterize this.

Using the fractional losses of 22%, 12% and the lead of Ref. [30], we calculate that the PA rate to the 2(1) $v = -5\ J = 1$ state, $|\Psi_+\rangle$, is $R_{PA}^+ = 1.9\ (0.8)\times10^6$ molecules/s and the PA rate to the 4(1) $v = -16\ J = 1$ state, $|\Psi_-\rangle$, is $R_{PA}^- = 1.1\ (0.5)\times10^6$ molecules/s. The ratio of PA strengths, R_{PA}^+/R_{PA}^-, is 1.83 (0.15). (Most of the error in the individual PA rates is correlated, so the uncertainty in this relative measurement is much less than the quadrature sum of the individual uncertainties.)

We can calculate the PA rate using a quantum perturbative framework [31]

$$R_{PA} = \left(\frac{3\lambda_{th}^2}{2\pi}\right)^{\frac{3}{2}} \frac{h}{2} n_{Li} n_{Rb} A_\Omega |\langle\Psi_S|\vec{d}|\Psi_{PA}\rangle|^2. \quad (4)$$

In Eq. (4), $|\Psi_S\rangle$ is the scattering wave function, λ_{th} is the thermal de Broglie wavelength, n_{Li} and n_{Rb} are the atom densities, and A_Ω are the radial factors for the two states and laser polarization. $|\Psi_{PA}\rangle$ is either $|\Psi_-\rangle$ or $|\Psi_+\rangle$, as given by Eqs. (1) or (2). Since none of the other nearby 4(1) vibrational levels have been observed in PA spectra, we assert that the cross section for PA to the deeply bound unperturbed $|\Psi_{4(1)}\rangle$ state is very small. The other various factors in Eq. (4) are the same for $|\Psi_+\rangle$ and $|\Psi_-\rangle$, so the relative PA rates are related approximately through

$$\frac{R_{PA}^+}{R_{PA}^-} = \frac{|\langle\Psi_S|\vec{d}|\Psi_+\rangle|^2}{|\langle\Psi_S|\vec{d}|\Psi_-\rangle|^2} \simeq \frac{c^2|\langle\Psi_S|\vec{d}|\Psi_{2(1)}\rangle|^2}{d^2|\langle\Psi_S|\vec{d}|\Psi_{2(1)}\rangle|^2} \simeq \frac{c^2}{d^2}. \quad (5)$$

Using $|c| = 0.84$ and $|d| = 0.53$ that we determined in Sec. III, we estimate that the ratio of the trap loss peaks should be $\frac{c^2}{d^2} = 2.5\ (0.6)$, which is indeed consistent with our trap loss data.

We next examine the decay of excited-state molecules to stable molecules, whose wave functions we designate $|\Psi_{v''}\rangle$. We write the decay strength as

$$\begin{aligned}B^+(v'') &= |\langle\Psi_{v''}|\vec{d}|\Psi_+\rangle|^2 = c^2|\langle\Psi_{v''}|\vec{d}|\Psi_{2(1)}\rangle|^2 \\ &\quad + 2cd|\langle\Psi_{2(1)}|\vec{d}|\Psi_{v''}\rangle\langle\Psi_{v''}|\vec{d}|\Psi_{4(1)}\rangle| \\ &\quad + d^2|\langle\Psi_{v''}|\vec{d}|\Psi_{4(1)}\rangle|^2, \quad (6)\end{aligned}$$

and

$$\begin{aligned}B^-(v'') &= |\langle\Psi_{v''}|\vec{d}|\Psi_-\rangle|^2 = d^2|\langle\Psi_{v''}|\vec{d}|\Psi_{2(1)}\rangle|^2 \\ &\quad - 2cd|\langle\Psi_{2(1)}|\vec{d}|\Psi_{v''}\rangle\langle\Psi_{v''}|\vec{d}|\Psi_{4(1)}\rangle| \\ &\quad + c^2|\langle\Psi_{v''}|\vec{d}|\Psi_{4(1)}\rangle|^2, \quad (7)\end{aligned}$$

where $\langle\Psi_{v''}|\vec{d}|\Psi_{2(1)}\rangle$ and $\langle\Psi_{v''}|\vec{d}|\Psi_{4(1)}\rangle$ are the dipole transition matrix elements connecting the v'' vibrational state of $X\,^1\Sigma^+$ or $a\,^3\Sigma^+$ to the bare 2(1) $v = -5$ and 4(1) $v = -16$ states.

Not shown in these equations are (1) an overall normalization factor, or (2) Hönl-London factors. The Hönl-London factors are based on the angular momenta of the excited and final states which are identical for the decay from the 2(1) state and the 4(1) state and will cancel in the ratio. The ratio of these decay strengths becomes

$$\frac{B^+(v'')}{B^-(v'')} \simeq \frac{c^2\,\mathcal{R}^2(v'') + 2cd\mathcal{R}(v'') + d^2}{d^2\,\mathcal{R}^2(v'') - 2cd\mathcal{R}(v'') + c^2}, \quad (8)$$

where $\mathcal{R}(v'') = \langle\Psi_{v''}|\vec{d}|\Psi_{2(1)}\rangle / \langle\Psi_{v''}|\vec{d}|\Psi_{4(1)}\rangle$ is the ratio of the dipole transition matrix elements.

We determine this ratio $B^+(v'')/B^-(v'')$ for individual final states from the REMPI and trap loss spectra, and give three examples in Table II. R_{CM}^- and R_{CM}^+ (column 2) are the cold molecule formation rates observed in REMPI in Fig. 2(a) when the PA laser is tuned to the $|\Psi^-\rangle$ or $|\Psi^+\rangle$ peak. There we observed that approximately twice as many molecules were formed in deeply bound singlet states when photoassociating to $|\Psi_-\rangle$ compared to $|\Psi_+\rangle$ [this is difficult to see in Fig. 2(a) because of saturation effects]. The cold molecule formation rate R_{CM} is related to the PA rate R_{PA} through $R_{CM} = R_{PA} \times B(v'')$. Using $R_{PA}^+/R_{PA}^- = 1.83$, as discussed above, we determined the relative decay strength $B^+(v'')/B^-(v'')$ for spontaneous decay to one of the vibrational states of $X\,^1\Sigma^+$ or $a\,^3\Sigma^+$ (column 3 in this table). We solve Eq. (8) for the ratio of transition moments $\mathcal{R}(v'')$, using $|c/d|^2 = 2.5$, and list these values in Table II as well. We show here only one of the solutions for $\mathcal{R}(v'')$. The other root is a value of order 2, which seems unreasonable since other unmixed 2(1) resonances lead to relatively small numbers of stable molecules.

Finally, we examine the decay strength $B^+(v'')$ and $B^-(v'')$, as computed using Eqs. (6) and (7). We show each of the terms within these equations individually in Table II. Recall that we have omitted an overall normalization in these terms, as we are only examining their relative sizes. There are some notable features to these results. First, in any of the examples shown, for either of the PA resonances, the $|\langle\Psi_{v''}|\vec{d}|\Psi_{4(1)}\rangle|^2$ contribution is the most significant, while the $|\langle\Psi_{v''}|\vec{d}|\Psi_{2(1)}\rangle|^2$ contribution is insignificantly small. Second, the cross term $2cd\mathcal{R}(v'')$ makes a strong (secondary) contribution to each term. This cross term contribution is of opposite sign for the two PA resonances. That is, if it adds to the decay strength of the Ψ_- resonance, it diminishes the decay strength of the Ψ_+ resonance. Finally, observing the relative magnitudes of these terms, we note that the cross term is approximately half the magnitude of the strong $|\langle\Psi_{v''}|\vec{d}|\Psi_{4(1)}\rangle|^2$ contribution for the Ψ_+ resonance, strongly reducing this decay path. This is consistent with our observations, in which we note very low generation of $X\,^1\Sigma^+$ or $a\,^3\Sigma^+$ molecules when tuned to the $|\Psi_+\rangle$ PA peak.
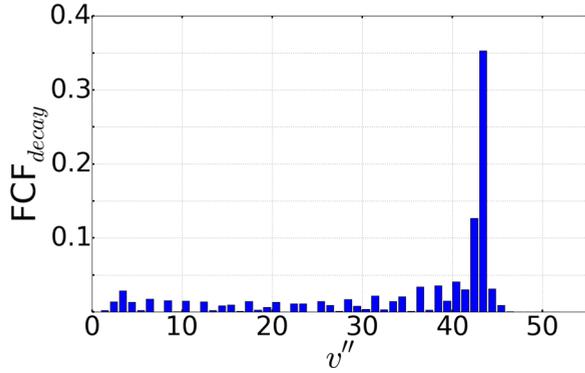
FIG. 4. Calculated Franck-Condon factors using PECs from Ref. [29] with assistance from LEVEL 8.0 [33] for the decay path from the PA state, $4(1) v = -16$, to $X\,^1\Sigma^+ v''$. Notice the maximum, $v'' = 43$.

A simple conceptual model that summarizes this analysis is thus. There is a fixed relative phase between the 4(1) and 2(1) vibrational wave functions that leads to constructive interference in the $|\Psi_-\rangle$ decay path and destructive interference in the $|\Psi_+\rangle$ decay path. A similar scenario was observed in NaK in coupled $(3)\,^3\Pi$ and $(3)\,^1\Pi$ states [32].

V. DECAY FROM 4(1) PA RESONANCE

In Sec. IV, we showed that photoassociating Li and Rb atoms through the $|\Psi_-\rangle$ resonance leads with high probability to stable molecules, primarily in the $X\,^1\Sigma^+$ electronic ground state. Here we discuss the distribution of this $X\,^1\Sigma^+$ electronic ground-state population.

We show in Fig. 4 the calculated Franck-Condon factors for the spontaneous decay of the $4(1) v = -16$ state to the various v'' levels of the $X\,^1\Sigma^+$ state. We calculated these FCFs using PECs from Ref. [29] and LEVEL 8.0 [33]. This plot suggests that the $v'' = 43$ level is the most highly populated, with a FCF of 0.35, and shows a secondary but still significant FCF of 0.13 for the $v'' = 42$ level. A broad pedestal of vibrational levels down to $v'' = 2$ are also populated to a lesser degree. Our observations here are in agreement with the calculated FCFs. We used a second dye, LDS 698, which lases from 14050-15050 cm^{-1}, to study population in $v'' = 38$-45. We observed very strong population of $v'' = 43$ and to a lesser

extent $v'' = 42$. Our RE2PI data on $v'' = 42$ and 43 will be presented elsewhere [19]. Unfortunately, direct comparison of that data to the REMPI data presented in this work on deeply bound vibrational levels is difficult. The two different dyes have different powers and modeling RE2PI is very difficult (modeling REMPI isn't any easier). Additionally the intermediate state for that work, $C\,^1\Sigma^+$, does not have a good theoretical model, so FCFs for the $C\,^1\Sigma^+ \leftarrow X\,^1\Sigma^+$ transition are unreliable, further complicating matters. At this point in time, our best estimate for the production rate of $v'' = 43$ is $R_{v''=43} = R_{PA}^- FCF_{43}(1.15c^2) = 3\times10^5$ molecules/s. The factor 1.15 represents the enhancement factor for bound state decay discussed in Sec. IV. This production rate is quite large and we expect that it could be increased further by increasing the PA power or MOT sizes.

To explore the deeply bound vibrational levels populated after PA through the 2(1)–4(1) mixed states, we used REMPI and RE2PI with the R590 dye which lases from 17050 to 18150 cm^{-1}. We show a typical REMPI scan in Fig. 5. In this spectrum, we scan ν_c, the REMPI or RE2PI laser frequency, with the PA laser locked to the $4(1) v = -16 J = 1$ line. We have observed most of these REMPI lines previously in our studies of photoassociation through other vibrational lines of the 2(1) and 4(1) series [21,27]. Our current focus is finding population of low-lying vibrational levels. For example, we have marked the series $B\,^1\Pi v' \leftarrow v'' = 2$ transitions with black dashed vertical lines in Fig. 5. The global maximum occurs at $v' = 14 \leftarrow v'' = 2$ (not shown). The progression provides strong evidence of population of the $v'' = 2$ vibrational state.

In contrast, population of the $v'' = 0$ vibrational state is difficult to observe in the RE2PI spectra of Fig. 5. The $4(1) v = -16 J = 1$ state decays weakly to the ground vibrational state, predicted to be around 100 molecules/s, compared to other vibration levels such as $v'' = 2$, predicted to be around 2×10^4 molecules/s. Furthermore, the candidate lines in Fig. 5 that might originate from the $v'' = 0$ vibrational state, labeled by green solid lines, are obscured by nearby stronger lines. For example, the $B\,^1\Pi v' = 2 \leftarrow v'' = 0$ transition is much weaker than it looks on Fig. 5 because it is right next to a much stronger $v'' = 4$ RE2PI transition. In order to identify these weak lines we have employed a form of depletion spectroscopy [34], in which we introduce a cw laser beam tuned to a $A\,^1\Sigma^+ v' \leftarrow X\,^1\Sigma^+ v''$ transition [19]. For these
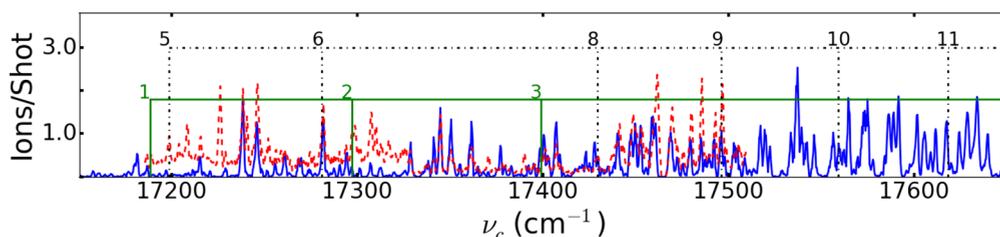

FIG. 5. REMPI (blue solid) and RE2PI (red dashed) scan; the PA laser was locked to the $4(1) v = -16 J = 1$ line. Black numbers and dot-dashed lines label $B\,^1\Pi v' \leftarrow v'' = 2$ transitions while green numbers and solid lines label $B\,^1\Pi v' \leftarrow v'' = 0$ transitions. No transitions from $v'' = 43$ show up in our REMPI (or RE2PI) data taken with the R590 dye. All transitions observed can be assigned to $X\,^1\Sigma^+ v'' = 0-20$ and $a\,^3\Sigma^+ v'' = 6-13$. The RE2PI data is necessary because for deeply bound initial states ionization by REMPI is out of range energetically. For example, $v' = 1, 2, 3 \leftarrow v'' = 0$ and $v' = 5 \leftarrow v'' = 2$ on this plot would not be observable without RE2PI (even though there are nearby visible peaks in REMPI).
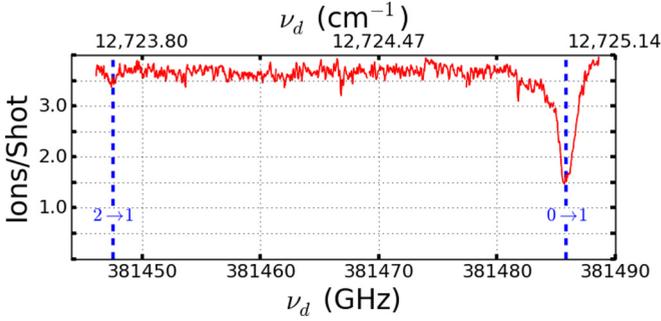
FIG. 6. Example of a depletion spectrum on the $v'' = 2$ state. For this spectrum, the REMPI laser was tuned to the $B\,^1\Pi\ v' = 14 \leftarrow v'' = 2$ transition, the PA laser was locked to the 4(1) $v = -16\ J = 1$ line, and ν_d, the frequency of the depletion laser, was scanned. Labeling is $J'' \rightarrow J'$. Our observed $v'' = 2$ rotational constant, $B_{v''} = 6.38$ GHz, matches the previous measurement [28].

measurements, we use the 150 mW ECDL to photoassociate the molecules, and the more tunable Ti:sapphire laser to drive the depletion transition. The PA and depletion beams copropagate, and are focused to a 200 μm diameter spot size in the MOT region. To benchmark this technique, we first applied it to a $v'' = 2$ resonance with the result shown in Fig. 6. For this spectrum, we tuned the REMPI laser frequency to the $B\,^1\Pi\ v' = 14 \leftarrow v'' = 2$ transition, and tuned ν_d, the depletion laser frequency, across the $A\,^1\Sigma^+\ v' = 15 \leftarrow v'' = 2$ transition. When on a depletion resonance, the initial state population available for ionization is transferred into a state not active in the REMPI process, thereby diminishing the REMPI signal. Compared to REMPI, depletion spectra are sparse and have narrow peak widths, in this case $\sim$1 GHz, a typical linewidth for this type of measurement at this intensity [11].

In Fig. 7, we show depletion of a $v'' = 0$ line. For this depletion spectrum, we tuned the RE2PI laser to the $B\,^1\Pi\ v' = 3 \leftarrow v'' = 0$ transition, and varied ν_d, the depletion laser frequency, through the $A\,^1\Sigma^+\ v' = 10,\ J' = 1 \leftarrow v'' = 0,\ J'' = 0$ transition. Each data point is the average of 10 measurements of the total ion count accumulated over 100 laser pulses, and error bars show the 1σ standard deviation of the mean. We fitted our depletion data to a Lorentzian line shape with a commercial
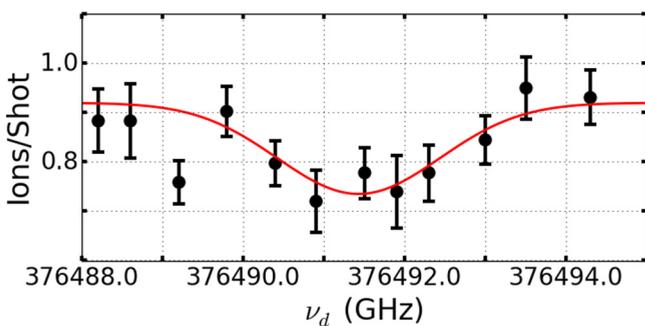

FIG. 7. Evidence of $X\,^1\Sigma^+\ v'' = 0\ J'' = 0$ population. Depletion spectra of the $A\,^1\Sigma^+\ v' = 10\ J' = 1 \leftarrow v'' = 0\ J'' = 0$ transition. The PA laser is locked to the 4(1) $v = -16\ J = 1$ peak; the RE2PI laser was tuned to the $B\,^1\Pi\ v' = 3 \leftarrow v'' = 0$ transition shown in Fig. 5. Here we extract a depletion of 0.19 (0.04) ions/shot.

TABLE III. Permanent dipole moment d (in Debye) in the ground state [39], generation rates $R_{v''=0}$ (in molecules/s), and rotational state J'' of the $v'' = 0$ ground state of bi-alkali diatomic molecules, as reached by PA followed by spontaneous emission. "n.s." indicates that this quantity is not specified.

Molecule	d	J''	$R_{v''=0}$	Ref.
RbCs	1.2	n.s.	500	[40]
		0	2000	[12]
LiCs	5.5	0	100	[11]
		2	5000	
NaCs	4.6	1	1×10^4	[13]
		0–4	1×10^5	[16]
KRb	0.6	n.s.	5000	[10]
LiRb	4.1	0	300	This work

fitting program, extracting the height of the Lorentzian to be -0.19 (0.04) ions/shot. The data in Fig. 7 clearly shows population in the ground state $v'' = 0$ vibrational level.

We have two ways to estimate the $v'' = 0\ J'' = 0$ production rate. First, we measured the PA rate and calculated the branching ratio. This gives us a $v'' = 0\ J'' = 0$ production rate of 70 (50) molecules/s [35]. Second, we measured the cold ion production rate in REMPI. To get the cold molecule production rate: $R_{CM} = \frac{N}{\tau \epsilon_d P_{\text{ion}}}$, we estimate τ, the transit time in the REMPI beam [36], to be 10 (5) ms, ϵ_d, the detector efficiency, to be about 50 (20)%, and P_{ion}, the ionization probability, to be about 5^{+10}_{-4}%, which gives us a generation rate of 600 molecules/s. Due to the large uncertainties in τ, ϵ_d, and P_{ion}, the uncertainty of R_{CM} is comparable to its magnitude. While none of the quantities in this estimate are very exact, the uncertainty in P_{ion} dominates and could fall anywhere between 1% and 15% (or even larger). Within the uncertainties, these two estimates of the production rate agree and we report the average, rounded to the nearest digit, 300 molecules/s.

In comparison to other experiments which generate $v'' = 0$ $J'' = 0$ by spontaneous decay, this rate is competitive, as shown in Table III. We consider both the generation rate and the dipole moments here. Because the applications for dipolar molecules rely on the dipole-dipole interaction, molecules with a large dipole moment are preferable. In KRb, an impressive 5000 molecules/s (in an unspecified rotational distribution) can be produced [10]; however the dipole moment, 0.57 Debye (D) [7], is very small compared to 4.1 D for LiRb. Likewise, RbCs can be produced at around 2000 molecules/s [12], but RbCs also has a small dipole moment at 1.2 D [37]. LiCs is produced at 100 molecules/s [11], but has a larger dipole moment of around 5.5 D [38]. Finally, NaCs is produced at 10^4 molecules/s [13], the highest rate, and has a large dipole moment at 4.6 D [39], but these are all in $J'' = 1$. Overall, LiRb has a good mix of a strong dipole moment and good generation rate.

VI. OUTLOOK

Our production rate of $v'' = 43\ J'' = 0$ is nearly three orders of magnitude larger than our $v'' = 0\ J'' = 0$ production rate, at 2×10^5 molecules/s. This is not the highest production of a single rovibrational level among bi-alkalis (or even in LiRb), but $v'' = 43$ is sufficiently bound that a STIRAP

transfer to the rovibronic ground state will not be too difficult. Here, we recommend using the $C\,^1\Sigma^+\,v'=22$ as the intermediate state based on calculated FCFs [41]. The "up" laser for this transfer is at 730 nm and the "down" laser is at 516 nm, both of which are covered by commercially available diode lasers. Additionally, this STIRAP transfer will be several orders of magnitude stronger than transfers used for KRb [7]. We predict (based on FCFs) that the transition dipole moment for each leg will be around 0.1 ea_0. This is a huge advantage because it reduces the requirement for stability of the two STIRAP lasers, reducing the experimental and complexity cost considerably. With this type of STIRAP transfer, similar to the continuous process reported in Ref. [42], we conservatively estimate producing 1×10^5 rovibronic ground-state molecules/s.

VII. CONCLUSION

We have experimentally explored 2(1)-4(1) mixing that allows PA to a deeply bound 4(1) state. From the sponta-

neous decay of our 4(1) $v=-16$ $J=1$ PA resonance, we present an observation of $X\,^1\Sigma^+\,v''=0$ in LiRb produced at $\sim$300 molecules/s. We have presented plans for increasing the rovibronic ground-state production rate by three orders of magnitude. Currently, work is underway in our laboratory to study bound-to-bound transitions in LiRb with depletion spectroscopy using this PA resonance. We will use the spectroscopic data to increase our ground-state generation rate and devise a plan to trap ground-state molecules.

[1] D. DeMille, Phys. Rev. Lett. **88**, 067901 (2002).

[2] K.-K. Ni, S. Ospelkaus, D. Wang, G. Quéméner, B. Neyenhuis, M. De Miranda, J. Bohn, J. Ye, and D. Jin, Nature (London) **464**, 1324 (2010).

[3] R. Krems, B. Friedrich, and W. C. Stwalley, *Cold Molecules: Theory, Experiment, Applications* (CRC Press, Boca Raton, FL, 2009).

[4] C. Trefzger, C. Menotti, and M. Lewenstein, Phys. Rev. Lett. **103**, 035304 (2009).

[5] B. Capogrosso-Sansone, C. Trefzger, M. Lewenstein, P. Zoller, and G. Pupillo, Phys. Rev. Lett. **104**, 125301 (2010).

[6] G. Pupillo, A. Griessner, A. Micheli, M. Ortner, D.-W. Wang, and P. Zoller, Phys. Rev. Lett. **100**, 050402 (2008).

[7] K.-K. Ni, S. Ospelkaus, M. De Miranda, A. Pe'er, B. Neyenhuis, J. Zirbel, S. Kotochigova, P. Julienne, D. Jin, and J. Ye, Science **322**, 231 (2008).

[8] C. M. Dion, C. Drag, O. Dulieu, B. Laburthe Tolra, F. Masnou-Seeuws, and P. Pillet, Phys. Rev. Lett. **86**, 2253 (2001).

[9] H. K. Pechkis, D. Wang, Y. Huang, E. E. Eyler, P. L. Gould, W. C. Stwalley, and C. P. Koch, Phys. Rev. A **76**, 022504 (2007).

[10] J. Banerjee, D. Rahmlow, R. Carollo, M. Bellos, E. E. Eyler, P. L. Gould, and W. C. Stwalley, Phys. Rev. A **86**, 053428 (2012).

[11] J. Deiglmayr, A. Grochola, M. Repp, K. Mörtlbauer, C. Glück, J. Lange, O. Dulieu, R. Wester, and M. Weidemüller, Phys. Rev. Lett. **101**, 133004 (2008).

[12] C. Bruzewicz, M. Gustavsson, T. Shimasaki, and D. DeMille, New J. Phys. **16**, 023018 (2014).

[13] P. Zabawa, A. Wakim, M. Haruza, and N. P. Bigelow, Phys. Rev. A **84**, 061401 (2011).

[14] W. Stwalley, J. Banerjee, M. Bellos, R. Carollo, M. Recore, and M. Mastroianni, J. Phys. Chem. A **114**, 81 (2009).

[15] J. Kleinert, C. Haimberger, P. J. Zabawa, and N. P. Bigelow, Phys. Rev. Lett. **99**, 143002 (2007).

[16] A. Wakim, P. Zabawa, M. Haruza, and N. Bigelow, Opt. Express **20**, 16083 (2012).

[17] J. Kobayashi, K. Aikawa, K. Oasa, and S. Inouye, Phys. Rev. A **89**, 021401 (2014).

[18] M. Viteau, A. Chotia, M. Allegrini, N. Bouloufa, O. Dulieu, D. Comparat, and P. Pillet, Science **321**, 232 (2008).

[19] I. C. Stevenson, D. B. Blasing, Y. P. Chen, and D. S. Elliott, Phys. Rev. A **94**, 062503 (2016).

[20] S. Dutta, A. Altaf, J. Lorenz, D. Elliott, and Y. P. Chen, J. Phys. B **47**, 105301 (2014).

[21] A. Altaf, S. Dutta, J. Lorenz, J. Pérez-Ríos, Y. P. Chen, and D. Elliott, J. Chem. Phys. **142**, 114310 (2015).

[22] W. Ketterle, K. B. Davis, M. A. Joffe, A. Martin, and D. E. Pritchard, Phys. Rev. Lett. **70**, 2253 (1993).

[23] M. Korek, G. Younes, and S. Al-Shawa, J. Mol. Struct.: THEOCHEM **899**, 25 (2009).

[24] The designation $v=-16$ of the 4(1) state is only approximate.

[25] For convenience, we will continue to label these states 4(1)$v=-16$ and 2(1)$v=-5$, according to their major constituent.

[26] G. Herzberg, *Molecular Spectra and Molecular Structure, I. Spectra of Diatomic Molecules*, 2nd ed. (Krieger, Malabar, FL, 1989).

[27] J. Lorenz, A. Altaf, S. Dutta, Y. P. Chen, and D. S. Elliott, Phys. Rev. A **90**, 062513 (2014).

[28] S. Dutta, A. Altaf, D. Elliott, and Y. P. Chen, Chem. Phys. Lett. **511**, 7 (2011).

[29] M. Ivanova, A. Stein, A. Pashov, H. Knöckel, and E. Tiemann, J. Chem. Phys. **134**, 024321 (2011).

[30] S. Dutta, D. S. Elliott, and Y. P. Chen, Europhys. Lett. **104**, 63001 (2014).

[31] P. Pillet, A. Crubellier, A. Bleton, O. Dulieu, P. Nosbaum, I. Mourachko, and F. Masnou-Seeuws, J. Phys. B **30**, 2801 (1997).

[32] S. Eckel, S. Ashman, and J. Huennekens, J. Mol. Spectrosc. **242**, 182 (2007).

[33] R. J. Le Roy, J. Quant. Spectrosc. Radiat. Transfer **186**, 167 (2017).

[34] D. Wang, J.-T. Kim, C. Ashbaugh, E. E. Eyler, P. L. Gould, and W. C. Stwalley, Phys. Rev. A **75**, 032511 (2007).

[35] For this estimate, both the PA rate and FCF have about a 50% uncertainty.

[36] The transit time is the time the molecules remain in the REMPI ionization volume after formation.

[37] P. K. Molony, P. D. Gregory, Z. Ji, B. Lu, M. P. Köppinger, C. R. Le Sueur, C. L. Blackley, J. M. Hutson, and S. L. Cornish, Phys. Rev. Lett. **113**, 255301 (2014).

[38] J. Deiglmayr, A. Grochola, M. Repp, O. Dulieu, R. Wester, and M. Weidemüller, Phys. Rev. A **82**, 032503 (2010).

[39] M. Aymar and O. Dulieu, J. Chem. Phys. **122**, 204302 (2005).

[40] J. M. Sage, S. Sainis, T. Bergeman, and D. DeMille, Phys. Rev. Lett. **94**, 203001 (2005).

[41] As previously stated, FCFs for the $C\,^1\Sigma^+ \leftarrow X\,^1\Sigma^+$ are unreliable, so this state may change by a few vibrational numbers but we expect it to be close to the optimum state.

[42] K. Aikawa, D. Akamatsu, M. Hayashi, K. Oasa, J. Kobayashi, P. Naidon, T. Kishimoto, M. Ueda, and S. Inouye, Phys. Rev. Lett. **105**, 203001 (2010).